Analysis of sub-grid scale modeling of the ideal-gas equation of state in hydrogen–oxygen premixed flames

Guillaume Ribert, Pascale Domingo, Luc Vervisch

Analysis of sub-grid scale modeling of the ideal-gas equation of state in hydrogen-oxygen premixed flames

Guillaume Ribert[a,*], Pascale Domingo[a], Luc Vervisch[a]

[a] *CORIA, CNRS & Normandy University, INSA de Rouen Normandie, France*

Abstract

In large-eddy simulations (LES) of multicomponent and fully compressible flows, the spatially filtered pressure needs to be evaluated, i.e. the pressure averaged over a volume. The flow is non-homogeneous within this volume and the state relationship linking pressure, density, temperature and species mass fractions should not be applied directly to their values resolved on the LES mesh. In practice, the unresolved correlations between density, species and temperature are usually neglected to compute the filtered pressure from the resolved fields. Analyzing one-dimensional laminar and three-dimensional turbulent H_2/O_2 space-filtered flames under lean and stoichiometric conditions, it is observed that a large part of the error introduced by the linearization of the equation of state can be counterbalanced by expressing the mean molar weight of the mixture with the Reynolds filtered species mass fractions, instead of the density-weighted (Favre) mass fractions. A sub-grid scale closure for the remaining part of the unknown correlation is also proposed, which relies on a scale similarity assumption. Finally, an approximate deconvolution/filtering procedure is discussed to estimate the Reynolds filtered mass fractions from the density-weighted mass fractions, which are the transported quantities in LES flow solvers.

Keywords: Equation of state, Hydrogen, Large Eddy Simulation, Sub-grid scale modeling, Deconvolution

*Corresponding author
Email address: guillaume.ribert@coria.fr
(Guillaume Ribert)

1. Introduction

Modern computing facilities supporting well-resolved flow simulations allow us to revisit some classic modeling assumptions to better describe flow physics. In the simulations of turbulent flames, the modeling of the interactions between flow turbulence, thermodynamics and chemistry are a very sensitive point. Neglecting the effects induced by unresolved fluctuations of the species concentrations and of the temperature cannot be an option in the context of high-fidelity simulations. Along these lines, the treatment of the equation of state (EoS) in fully compressible large-eddy simulation (LES) just started to be addressed in the literature [1, 2, 3].

The filtering of the EoS provides the filtered pressure in a fully compressible LES. Correlations between species, mass fractions and temperature are usually neglected to simply express the filtered pressure directly from the knowledge of the density-weighted filtered species mass fractions and temperature. A formulation that may be valid is the case where a species concentration dominates the mixture, for instance nitrogen, but fails in the particular case of oxy-combustion. Even in the case of a binary mixture, it was illustrated in [4] how the error, due to linearization of the filtered EoS, grows with the filter size.

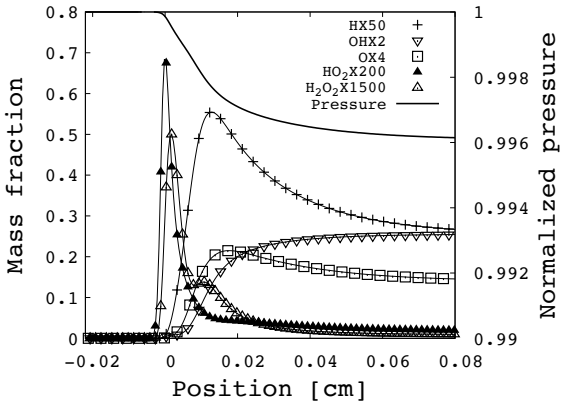

Figure 1: Minor species and pressure. One-dimensional stoichiometric ($\phi = 1$) H_2/O_2 freely propagating premixed flame.

This issue is further examined by filtering stoichiometric ($\phi = 1$) and fuel-lean ($\phi = 0.2$) one-dimensional freely propagating premixed H_2/O_2 flames and a three-dimensional fuel-lean turbulent slot burner, both simulated with detailed chemistry. The filtering of the EoS is analyzed, and modeling is discussed to significantly reduce the contribution of the unresolved sub-grid scale (SGS) part.

2. Problem formulation

The EoS for an ideal or non-ideal gas composed of n chemical species may be written in a generic form as a function of the partial densities, ρ_i, and the temperature T, *i.e.* $P = P(\rho_1, \cdots, \rho_n, T)$. For an ideal gas

$$P = R\left(\sum_{i=1}^{n} \frac{\rho_i}{W_i}\right) T = \rho R\left(\sum_{i=1}^{n} \frac{Y_i}{W_i}\right) T = \rho r_{\text{Mix}} T \,, \qquad (1)$$

where Y_i is the mass fraction and W_i is the molar weight of the i-th species. R is the universal gas constant and $r_{\text{Mix}} = \left(\sum_{i=1}^{n} Y_i/W_i\right) R = R/W$ the gas constant of the mixture and $W = (\sum_{i=1}^{n} Y_i/W_i)^{-1}$ the species averaged molar weight. The EoS is an algebraic functional relationship which holds for an homogeneous medium, however the LES cell is non-homogeneous. The filtered pressure reads

$$\overline{P} = R\left(\frac{\overline{\rho T Y_1}}{W_1} + \cdots + \frac{\overline{\rho T Y_n}}{W_n}\right) . \qquad (2)$$

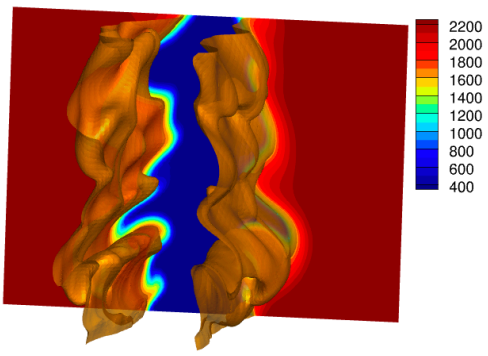

Figure 2: Snapshot of temperature [K] in the lean ($\phi = 0.2$) H_2/O_2 slot burner turbulent premixed flame. Iso-surface $T = 1680$ K.

Today, in most fully compressible flow solvers, it is assumed that correlations between species concentrations and temperature can be neglected when filtering

the EoS

$$\overline{\rho Y_i T} = \overline{\rho}\,\widetilde{Y_i T} \approx \overline{\rho}\,\widetilde{Y}_i\,\widetilde{T}\,, \tag{3}$$

where the usual Favre filtering is introduced ($\widetilde{T} = \overline{\rho T}/\overline{\rho}$ and $\widetilde{Y}_i = \overline{\rho Y}_i/\overline{\rho}$). This assumption may be valid when a diluent (usually nitrogen) dominates the gas composition, i.e., $Y_{N_2} >> Y_i\ \forall i \neq N_2$. Then the dominant nitrogen term assumes in Eq. (2) that $\overline{P} \approx \overline{\rho T} R(\widetilde{Y}_{N_2}/W_{N_2}) = \overline{\rho} r_{\mathrm{Mix}} \widetilde{T}$, with $r_{\mathrm{Mix}} = R(\widetilde{Y}_{N_2}/W_{N_2})$ roughly constant. This assumption of weak variations of the mean molar weight may not be valid on the rich side of non-premixed airflames or at any flow location in the case of oxy-flames. In most low-Mach number codes, however, the background pressure is set to a constant when computing the density, so the EoS filtering issue does not really exist aside from fully compressible simulations.

3. Flame configurations and numerics

Two canonical flame configurations are examined to study space filtering of the EoS. The fully compressible SiTCom-B flow solver is used, in which the convective terms are computed resorting to a fourth-order centered skew-symmetric-like scheme [5], the diffusive terms are discretized with a fourth-order centered scheme, time is advanced with a third-order Runge-Kutta method [6] and the boundary conditions are prescribed with 3D-NSCBC [7]. This code has been validated for both DNS and LES [8, 9, 10, 11, 12, 13].

The first are one-dimensional premixed flames freely propagating in lean ($\phi = 0.2$) or stoichiometric ($\phi = 1$) mixtures of H_2/O_2. The chemistry is described for eight species, O_2, H_2, H_2O, H, OH, O, HO_2, H_2O_2, involved in 21 elementary reactions [14]. The transport coefficients are expressed with the Curtiss and Hirschfelder formulation [15]. For a resolution of 5 μm, Fig. 1 shows the distribution of minor species and pressure across the stoichiometric flame. The flame speeds are S_L = 10.1 m/s ($\phi = 1$) and 2.6 m/s ($\phi = 0.2$). The characteristic thermal flame thickness is 200 μm for the stoichiometric flame and 244 μm for the lean flame.

The second is a three-dimensional turbulent premixed flame ($\phi = 0.2$) developing downstream of a slot burner (Figure 2). Results for the corresponding stoichiometric case are provided in the supplemental material. The bulk velocity of the premixed jet is 70 m/s and its temperature is 300 K. The temperature of the coflowing burnt gases is 2280 K and the bulk velocity of this stream is 15 m/s. Velocity fluctuations are added to the injected mean flow, according to a synthetic homogeneous turbulence with $u'/S_L = 8$. The lengths of the computational domain of the spatially developed simulation are: 4 mm × 5 mm × 4 mm and the jet thickness is 1 mm, featuring a slot width of 0.3 mm. The turbulence Reynolds number at inlet is about 30, the Damköhler number is 0.102 and the Karlovitz number 55.5. The structured mesh is composed of 560M cells with a resolution of 5 μm.

4. Analysis of EoS filtering

Expressing the EoS in the linearized form, as usually done,

$$\overline{P} = R\left(\frac{\overline{\rho}\widetilde{T}\,\widetilde{Y}_1}{W_1} + \cdots + \frac{\overline{\rho}\widetilde{T}\,\widetilde{Y}_n}{W_n}\right), \tag{4}$$

implies that the SGS contribution

$$R\sum_{i=1}^{n}\frac{\overline{\rho T Y_i} - \overline{\rho}\widetilde{T}\,\widetilde{Y}_i}{W_i} \tag{5}$$

stays small compared with the filtered pressure.

Filtered quantities are obtained in the one-dimensional flame and the three-dimensional DNS by applying an approximate and discretized form of a Gaussian filter of size Δ [16, 17]

$$\overline{Y}_i = Y_i + \frac{\Delta^2}{24}\nabla^2\overline{Y}_i\,, \tag{6}$$

in which an implicit formulation is chosen to secure stability and facilitate deconvolution introduced thereafter.

Figure 3 shows the distribution through the one-dimensional flames of

$$R\,\frac{\overline{\rho T Y_i} - \overline{\rho}\widetilde{T}\,\widetilde{Y}_i}{W_i} \times \frac{1}{\overline{\overline{P}}} \tag{7}$$

for every species and its sum over all the chemical species. The filter size is Δ = 300 μm, which is representative of those used for LES in complex geometries. H_2O, H, OH and O have a positive contribution to the SGS term, at $\phi = 1$ up to 12% (6% at $\phi = 0.2$) for H_2O while other species of this group contribute less than 5%. The SGS term of HO_2 and H_2O_2 is of the order of a few % with a change of sign across the reaction zone. O_2 and H_2 have a negative SGS contribution, reaching for the stoichiometric flame ($\phi = 1$) -7% and -15% (-3% and -6% at $\phi = 0.2$), respectively. Overall, the sign of the SGS term seems to depend on the

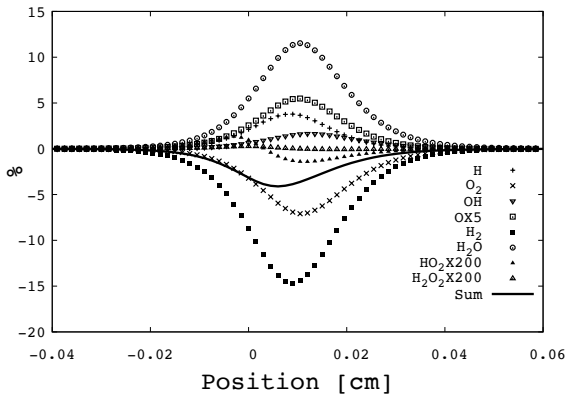

(a) $\phi = 1$

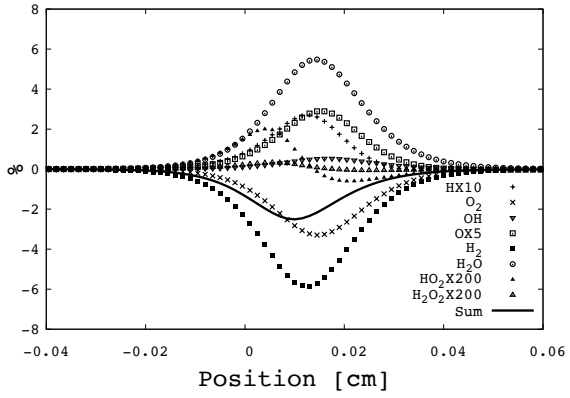

(b) $\phi = 0.2$

Figure 3: Distribution of $R(\overline{\rho T Y_i} - \overline{\rho}\widetilde{T}\,\widetilde{Y}_i)/(W_i\overline{P})$ (%) in a one-dimensional flame. *A-priori* filtering with a filter size $\Delta = 300$ µm.

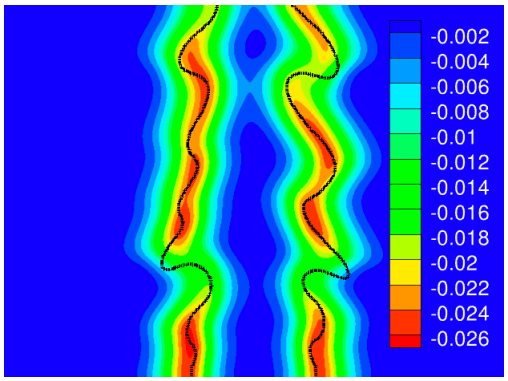

Figure 4: $P^{\star}_{\mathrm{SGS_{EoS}}} = \left(\overline{P} - \overline{\rho}R\widetilde{T}\sum_i(\widetilde{Y}_i/W_i)\right)/\overline{P}$. Snapshot in a transverse plane. Black line: iso-progress variable at 0.7. Filter size $\Delta = 480$ µm.

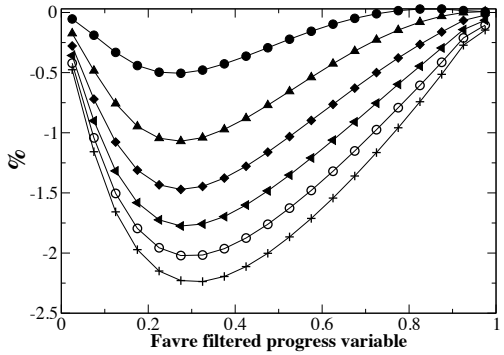

Figure 5: $\left\langle P^{\star}_{\mathrm{SGS_{EoS}}} \middle| \widetilde{c} \right\rangle$ with filter size •: $\Delta = 80$ µm, ▲: 160 µm, ♦: 240 µm, ▼: 320 µm, ∘ : 400 µm, +: 480 µm.

correlation between the species and the heat release rate (positive for products and negative for reactants). The sum over all species is of the order of -4% at $\phi = 1$ and -2.6% at $\phi = 0.2$.

The pressure variation expected through the laminar flame may be scaled from the conservation of mass and momentum, leading to

$$\frac{\Delta P}{P_{\mathrm{o}}} = \left(\frac{\rho_{\mathrm{o}}}{\rho_{\mathrm{b}}} - 1\right)\frac{\rho_{\mathrm{o}} S_{\mathrm{L}}^2}{P_{\mathrm{o}}}\,, \tag{8}$$

where the subscripts 'o' and 'b' denote fresh and burnt gases, respectively. In accordance with the one-dimensional flame simulation, a variation of the pressure of 0.39% is expected through the H_2/O_2 stoichiometric flame (Figure 1). Therefore, the error brought by the linearization of the EoS is of the order of 10 times the flame pressure jump, which would significantly alter the quality of a simulation (a similar observation is made for $\phi = 0.2$).

Figure 4 shows a snapshot of

$$P^{\star}_{\mathrm{SGS_{EoS}}} = \left(\overline{P} - \overline{\rho}R\widetilde{T}\sum_i \frac{\widetilde{Y}_i}{W_i}\right) \times \frac{1}{\overline{P}} \tag{9}$$

in a transverse plane of the slot burner three-dimensional flame ($\phi = 0.2$) for $\Delta = 480$ µm. As in the one-dimensional flame, the normalized SGS contribution peaks at -2.6%. The amplitude of this SGS part does not seem to be strongly correlated with flame curvature. The mean of the same SGS quantity conditioned on values of the filtered progress variable $\widetilde{c}$, for filter sizes varying between 80 µm and 480 µm, is plotted in Figure 5. The

progress variable is defined as $\widetilde{c} = \widetilde{Y}_{H_2O}/Y_{H_2O,\text{bunrt}}$. The amplitude of the conditional mean of the SGS contribution confirms its order of magnitude, which grows with the filter size, with larger values on the fresh gas side (peak at −2.25% for $\Delta = 480$ μm).

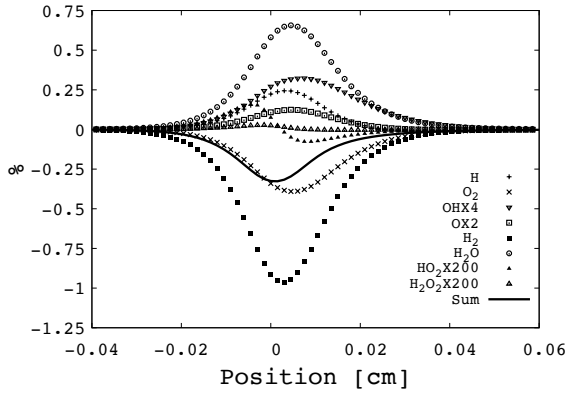

(a) $\phi = 1$

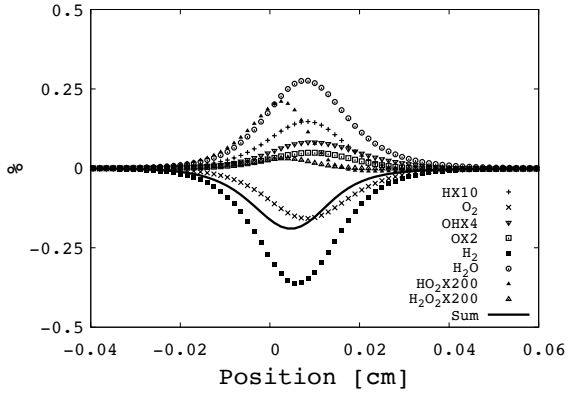

(b) $\phi = 0.2$

Figure 6: Normalized contribution (%) of the i-th species and of the sum of the species to the SGS EoS for $R(\overline{\rho T Y_i} - \overline{\rho}\widetilde{T}\,\widetilde{Y}_i)/(W_i\overline{P})$. One-dimensional flame *a priori* filtering with filter size $\Delta = 300$ μm.

5. SGS modeling of the EoS

Equation (3) hypothesizes that correlations between temperature and species remain moderate and also that density-weighted averaging could be applied to both Y_i and T, even though the density appears only once in the filtered expression. Relaxing the latter hypothesis leads to

$$\overline{P} = R\left(\frac{\overline{\rho}\widetilde{T}\,\widetilde{Y}_1}{W_1} + \cdots + \frac{\overline{\rho}\widetilde{T}\,\widetilde{Y}_n}{W_n}\right) \qquad (10)$$

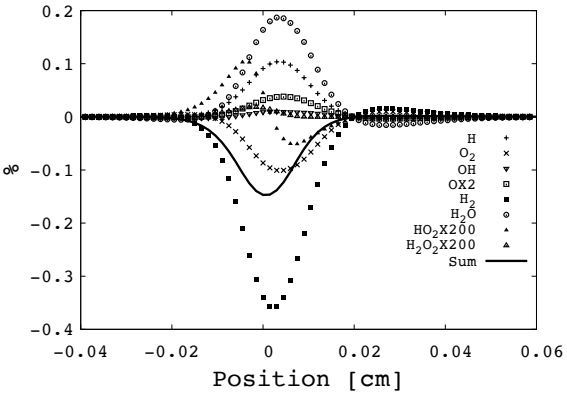

(a) $\phi = 1$

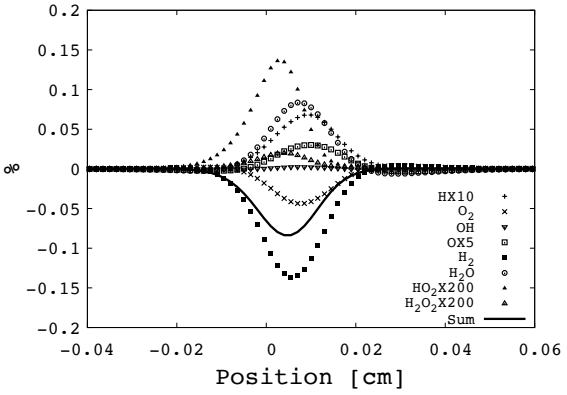

(b) $\phi = 0.2$

Figure 7: Normalized contribution (%) of the i-th species and of the sum of the species to the SGS EoS for $R(\overline{\rho T Y_i} - \overline{\rho}\widetilde{T}\,\widetilde{Y}_i - (\overline{\overline{\rho}\widetilde{T}\,\widetilde{Y}_i} - \overline{\overline{\rho}}\overline{\widetilde{T}}\,\overline{\widetilde{Y}}_i))/(W_i\overline{P})$. One-dimensional flame *a priori* filtering with filter size $\Delta = 300$ μm.

where $\overline{Y}_i$ has replaced $\widetilde{Y}_i$. The corresponding normalized SGS term

$$R\,\frac{\overline{\rho T Y_i} - \overline{\rho}\widetilde{T}\,\widetilde{Y}_i}{W_i} \times \frac{1}{\overline{P}}\,, \qquad (11)$$

is examined for all species in Figure 6 for the one-dimensional flames. In the stoichiometric flame, the SGS contribution for H_2O and H_2 now peaks at 0.66% (0.27% for $\phi = 0.2$) and -0.96% (-0.375% for $\phi = 0.2$), respectively. Compared to Figure 3, where 12% and 15% were reported for $\phi = 1$, the reduction brought by the use of Reynolds averaging for the mass fractions is significant. Similarly, the total contribution is reduced to -0.3% with the Reynolds formulation (previously −4%).

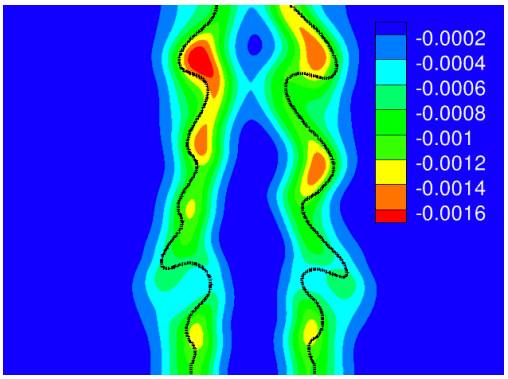

Figure 8: Snapshot in a transverse plane $P^{+}_{\mathrm{SGS_{EoS}}} = \left(\overline{P} - \overline{\rho} R \widetilde{T} \sum_i (\widetilde{Y}_i / W_i)\right) / \overline{P}$. 9. Black line: iso-progress variable at 0.7. Filter size 480 µm.

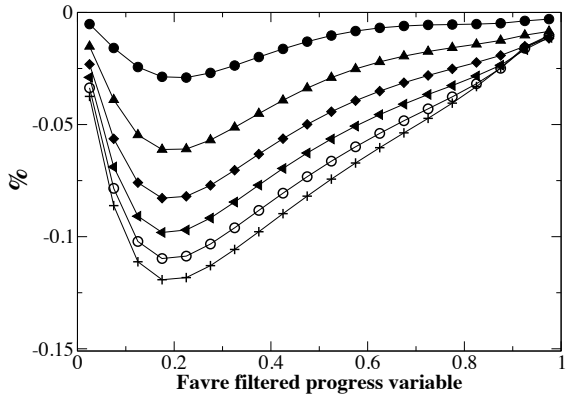

Figure 9: $\left\langle P^{+}_{\mathrm{SGS_{EoS}}} \middle| \widetilde{c} \right\rangle \times 100$ with filter size •: Δ = 80 µm, ▲: 160 µm, ♦: 240 µm, ▼: 320 µm, ∘ : 400 µm, +: 480 µm.

This is also the case at $\phi = 0.2$ where the total error is now at -0.20% (-2.6% previously).

To further reduce the departure between the filtered pressure and the pressure computed from filtered quantities, Leonard decomposition may be added to the species and temperature correlations [18]

$$\overline{\rho T Y_i} - \overline{\rho} \widetilde{T} \widetilde{Y}_i = \overline{\overline{\rho} \widetilde{T} \widetilde{Y}_i} - \overline{\overline{\rho}} \overline{\widetilde{T}} \overline{\widetilde{Y}_i} + \xi_i \,. \qquad (12)$$

Neglecting the unresolved term ξ_i leads to

$$\overline{P} = R \sum_i \left(\frac{\overline{\rho} \widetilde{T} \widetilde{Y}_i + \overline{\overline{\rho} \widetilde{T} \widetilde{Y}_i} - \overline{\overline{\rho}} \overline{\widetilde{T}} \overline{\widetilde{Y}_i}}{W_i} \right) . \qquad (13)$$

Following this modeling, the normalized remaining SGS term

$$\frac{R}{W_i} \left[\overline{\rho T Y_i} - \overline{\rho} \widetilde{T} \widetilde{Y}_i - \left(\overline{\overline{\rho} \widetilde{T} \widetilde{Y}_i} - \overline{\overline{\rho}} \overline{\widetilde{T}} \overline{\widetilde{Y}_i} \right) \right] \times \frac{1}{\overline{\overline{P}}} \qquad (14)$$

is seen for all species across the one-dimensional flames in Figure 7. SGS terms are further reduced, leading to a peak of 0.18% for H_2O and -0.35% for H_2. The peak of the sum of the error over the species is also reduced to -0.15% (was -4% with the Favre mass fractions and -0.3% with the Reynolds ones). This reduction is also observed for the lean flame ($\phi = 0.2$), with a sum of the error which now peaks at -0.08% (was -2.6% with the Favre and -0.20% with Reynolds). The most significant reduction of the error was such achieved when replacing the Favre species mass fractions (Eq. 4) by the Reynolds ones in the equation of state (Eq. 10).

Equation (10) with the Reynolds mass fractions is thus tested in the three-dimensional flame. Figure 8 shows a snapshot of $P^{+}_{\mathrm{SGS_{EoS}}}$, the departure between the filtered pressure and its estimation from Eq. (10)

$$P^{+}_{\mathrm{SGS_{EoS}}} = \left(\overline{P} - \overline{\rho} R \widetilde{T} \sum_i \frac{\overline{Y}_i}{W_i} \right) \times \frac{1}{\overline{\overline{P}}} \,. \qquad (15)$$

Compared to Figure 4, which features the usual expression for the pressure, the SGS term that would be neglected is reduced by more than an order of magnitude. The mean of this term conditioned on the density-weighted progress variable is seen in Figure 9, and the same trend is observed in the reduction of the part that would be left unresolved in a simulation.

The conditional mean of the pressure and of the pressure gradient in the direction normal to the flame surface are seen in Figs. 10 and 11. The usual expression of the pressure based on the density-weighted filtered mass fraction (dashed line) computed from the DNS misses the pressure response. The use of the Reynolds average (line with circle) captures the pressure. Notice that because the normalisation differs from the one used for $P^{+}_{\mathrm{SGS_{EoS}}}$, the errors seen in Fig. 10 are not exactly those of Fig. 9, even though the order of magnitude stays the same.

Aside from a-priori testing, in finite volume flow solvers, Rankine-Hugoniot type budgets are verified by construction and errors on the pressure are likely to compensate over the aerothermochemical variables whose balance equations are solved. Hence, LES with implicit filtering of the pressure would feature the ex-

pected gradient in the flame normal direction, thus avoiding responses as the dashed-line in Fig. 10. However, filtered DNS results suggest that this may not be the case in highly-refined simulations with explicit filtering, and one may also wish to achieve a better control of the distribution of the error in LES with implicit filtering. A strategy is now discussed to tackle this issue.

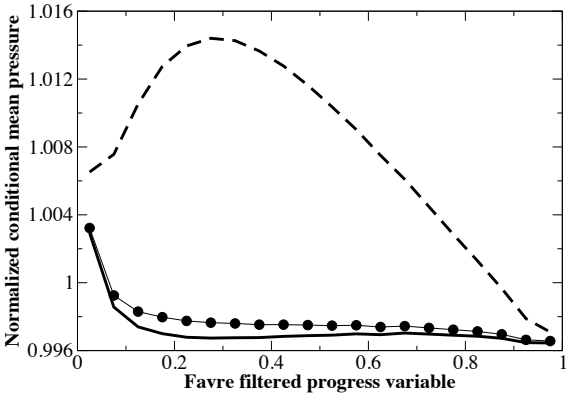

Figure 10: Conditional mean of pressure $\left\langle \overline{P}|\widetilde{c}\right\rangle / P_{\mathrm{o}}$. ——— : $\overline{P}$ from DNS, – – – – : $\overline{P} = \overline{\rho} R \widetilde{T} \sum_i (\widetilde{Y}_i / W_i)$, —•— : $\overline{P} = \overline{\rho} R \widetilde{T} \sum_i (\overline{Y}_i / W_i)$. $\Delta = 480$ µm.

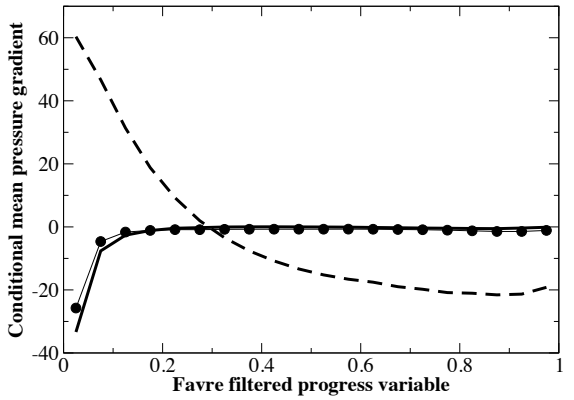

Figure 11: Conditional mean of pressure gradient $\left\langle \nabla \overline{P} \cdot \mathbf{n} | \widetilde{c} \right\rangle$. $\mathbf{n} = -\nabla \mathbf{c} / |\nabla \mathbf{c}|$: flame normal. ——— : $\overline{P}_{\mathrm{DNS}}$, – – – – : $\overline{\rho} R \widetilde{T} \sum_i (\widetilde{Y}_i / W_i)$, —•— : $\overline{\rho} R \widetilde{T} \sum_i (\overline{Y}_i / W_i)$. $\Delta = 480$ µm.

6. Toward LES with SGS modeling of EoS

Equation (10), which appears as a valuable expression for the filtered pressure in the case of multicomponent

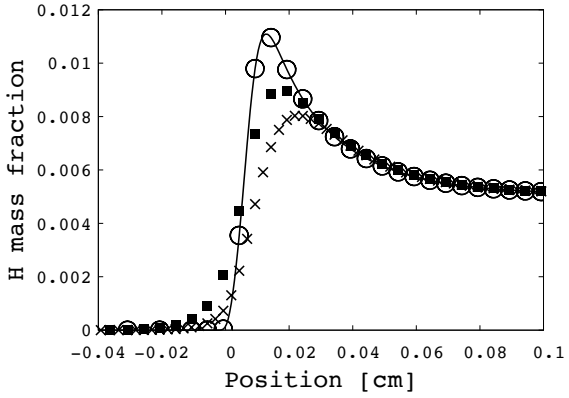

Figure 12: One-dimensional flame ($\phi = 1$) *a priori* filtering with filter size $\Delta = 300$ µm. ——— : Y_{H}. × : $\widetilde{Y}_{\mathrm{H}}$. ○ : Y_{H} from deconvolution. ■ : $\overline{Y}_{\mathrm{H}}$.

and fully compressible flows, requires the calculation of $\overline{Y}_i$, for which an equation is not solved since density-weighted quantities are usually considered in LES. Relations between $\widetilde{Y}_i$, the transported density weighted mass fractions, and $\overline{Y}_i$, their Reynolds counterpart have been derived in the Reynolds Average Navier Stokes (RANS) literature [19]. These relations are valid in the asymptotic limit of an infinitely thin flame separating fresh and burnt gases. In LES with complex chemistry, the flame signal must be resolved over the mesh and it cannot be reduced to a jump condition within the subgrid.

Approximate deconvolution under various conditions has been introduced to estimate unresolved terms from the knowledge of the information available on the mesh nodes [20, 17, 21, 10, 22]. Reversing the approximate Gaussian filtering operation of Eq. (6) brings the approximate deconvolution operator

$$\rho Y_i = \mathcal{L}_\Delta^{-1}[\overline{\rho}\widetilde{Y}_i] = \overline{\rho}\widetilde{Y}_i - \frac{\Delta^2}{24}\nabla^2(\overline{\rho}\widetilde{Y}_i)\,; \qquad (16)$$

then the Reynolds filtered mass fraction reads

$$\overline{Y}_i = \frac{\mathcal{L}_\Delta^{-1}[\overline{\rho}\widetilde{Y}_i]}{\mathcal{L}_\Delta^{-1}[\overline{\rho}]} + \frac{\Delta^2}{24}\nabla^2\overline{Y}_i\,. \qquad (17)$$

With this combination of an explicit formulation for deconvolution Eq. (16) and an implicit one for filtering (Eq. (17)), only derivatives of quantities resolved over the LES mesh are computed, thus avoiding the application of discretization operators to the deconvoluted

signals, which may not be fully resolved by the coarse mesh.

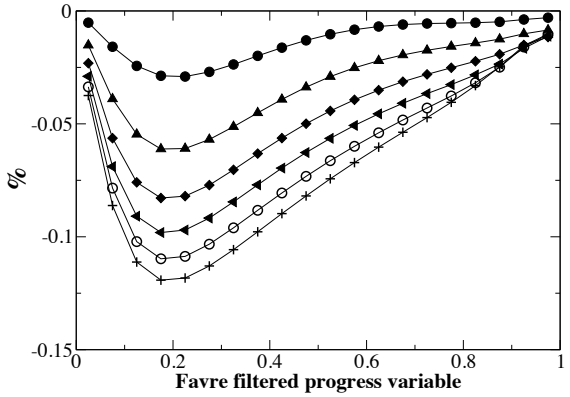

Figure 13: $\left\langle 1 - (\overline{\rho}R\widetilde{T}/\overline{P}) \sum_i \overline{\mathcal{L}_\Delta^{-1}[\overline{\rho}\widetilde{Y}_i]/(W_i\mathcal{L}_\Delta^{-1}[\overline{\rho}])}\middle|\widetilde{c}\right\rangle$ in %. Filter size •: Δ = 80 µm, ▲: 160 µm, ♦: 240 µm, ▼: 320 µm, ∘ : 400 µm, +: 480 µm.

This procedure is applied to the one-dimensional stoichiometric flame at first. Figure 12 shows the distribution of the mass fractions (original, density-weigthed filtered, deconvoluted and Reynolds filtered) for the H radical and Δ = 300 µm. The deconvolution at Δ perfectly recovers the original profiles from the density-weighted mass fraction and thus allows for computing the Reynolds filtered signal, which strongly differs from the density-weighted signal in the flame zone. Applied to the three-dimensional flame, the approximate deconvolution/filtering of the density-filtered quantities provides an estimation of the filtered pressure with an error of the order of -0.12% for the larger filter size (Figure 13), which is in line with the direct application of $\overline{Y}_i$ in the EoS reported in Figure 9. These departures of -0.12% should again be compared against those of -2.25% observed in Figure 5 using the EoS with the density-weighted mass fractions.

7. Summary

The filtering of the EoS, which provides the pressure in fully compressible simulations, has been discussed in the context of oxy-flames for which there is no species dominating the mean molar weight. Two H_2/O_2 reacting flows have been examined, including stoichiometric and fuel-lean one-dimensional freely propagating premixed flames and a three-dimensional fuel-lean turbulent slot burner. In these flames, *a priori* LES filtering has revealed that the filtered pressure was better approximated using the Reynolds filtered mass fractions of the species to compute the molecular weight of the mixture. A deconvolution procedure has then been set up and evaluated to estimate the Reynolds filtered mass fractions from the density-weighted transported mass fractions.

Acknowledgments

Part of this study was performed during the 2016 Summer Program of the Center for Turbulence Research, Stanford University, CA, USA. This work was granted access to the HPC resources of IDRIS, CCRT and CINES made by GENCI (Grand Equipement National de Calcul Intensif). The computing resources of CRIANN were also used.

References

[1] M. Masquelet, S. Menon, Y. Jin, R. Friedrich, Aerospace Sci. Tech. 13 (2009) 466–474.
[2] G. Ribert, X. Petit, P. Domingo, J. Supercritical Fluids 121 (2017) 78–88.
[3] U. Unnikrishnan, X. Wang, S. Yang, V. Yang, volume AIAA 2017-4855.
[4] L. Selle, N. Okong'o, J. Bellan, K. Harstad, J. Fluid Mech. 593 (2007) 57–91.
[5] F. Ducros, F. Laporte, T. Soulères, V. Guinot, P. Moinat, B. Caruelle, J. Comput. Phys. 161 (2000) 114–139.
[6] S. Gottlieb, C. Shu, Math. Comput. 67 (1998) 74–85.
[7] G. Lodato, P. Domingo, L. Vervisch, J. Comput. Phys 227 (2008) 5105–5143.
[8] P. Domingo, L. Vervisch, Combust. Flame 177 (2017) 109–122.
[9] L. Bouheraoua, P. Domingo, G. Ribert, Combust. Flame 179 (2017) 199–218.
[10] P. Domingo, L. Vervisch, Proc. Combust. Inst. 35 (2015) 1349–1357.
[11] P. Domingo, L. Vervisch, D. Veynante, Combust. Flame 152 (2008) 415–432.
[12] G. Lodier, C. Merlin, P. Domingo, L. Vervisch, F. Ravet, Combust. Flame 159 (2012) 3358–3371.
[13] C. Merlin, P. Domingo, L. Vervisch, Flow Turbulence and Combust. 90 (2013) 29–68.
[14] F. A. Williams, J Loss Prevent. Process Ind. 21 (2008) 131–135.
[15] C. F. Curtiss, J. O. Hirschfelder, J. Chem. Phy. 17 (1949) 550.
[16] P. Sagaut, Large Eddy Simulation for Incompressible Flows: An Introduction, Springer-Verlag, Berlin Heidelberg, 2nd edition, 2001.
[17] F. Katopodes, R. L. Street, M. Xue, J. H. Ferziger, J. Atm. Sci. 62 (2004) 2058–2077.
[18] M. Germano, Phys. Fluids 29 (1986) 2323.
[19] K. N. C. Bray, Symp. (Int.) on Combust. 26 (1996) 1–26.
[20] J. Mathew, Proc. Combust. Inst. 29 (2002) 1995–2000.
[21] S. T. Bose, P. Moin, Phys. Fluids 26 (2014) 015104.
[22] Z. Nikolaou, L. Vervisch, Flow Turbulence and Combust. 101 (2018) 33–53.